ADVANCED MATERIALS
www.advmat.de

Dual-Mode Hydrogels with Structural and Fluorescent Colors toward Multistage Secure Information Encryption

Yu Sun, Xiaoxia Le, Hui Shang, Ying Shen, Yue Wu, Qingquan Liu, Partick Théato, and Tao Chen**

Constructing an anti-counterfeiting material with non-interference dual optical modes is an effective way to improve information security. However, it remains challenging to achieve multistage secure information encryption due to the limited stimulus responsiveness and color tunability of the current dual-mode materials. Herein, a dual-mode hydrogel with both independently tunable structural and fluorescent colors toward multistage information encryption, is reported. In this hydrogel system, the rigid lamellar structure of poly(dodecylglyceryl itaconate) (pDGI) formed by shear flow-induced self-assembly provides the restricted domains wherein monomers undergo polymerization to form a hydrogel network, producing structural color. The introduction of fluorescent monomer 6-acrylamidopicolinate (6APA) as a complexation site provides the possibility of fluorescent color formation. The hydrogel's angle-dependent structural color can be controlled by adjusting the crosslinking density and water content. Additionally, the fluorescence color can be modulated by adjusting the ratio of lanthanide ions. Information of dual-mode can be displayed separately in different channels and synergistically overlayed to read the ultimate message. Thus, a multistage information encryption system based on this hydrogel is devised through the programed decryption process. This strategy holds tremendous potential as a platform for encrypting and safeguarding valuable and authentic information in the field of anti-counterfeiting.

1. Introduction

Counterfeiting is of global importance and has infiltrated various industries, posing significant threats to consumer safety, economy, and public health.[1,2] Therefore, it is essential to develop new anti-counterfeiting materials and technologies to meet the increasing challenges of counterfeiting. Up to now, materials with structural color or fluorescent color have attracted widespread attention in the anti-counterfeiting field due to their respective advantages.[3–6] For instance, structural color materials show vivid color under visible light and resist fading, while fluorescent materials emit multicolored fluorescence at specific excitation wavelengths.

Structural color materials can display bright colors under visible light due to their periodic micro- and nano-structures.[7–9] Typical structural color materials include photonic crystals,[10,11] cholesteric liquid crystals,[12–14] block copolymers,[15,16] or cellulose nanocrystals.[17–19] When these materials can change their distance between reflecting layers upon external stimulation, i.e., they could be "activated", it renders these materials useful for information encryption.[20,21] As another effective anti-counterfeiting material, fluorescent materials that contain emitting sources (e.g., carbon dots,[22–24] dyes,[25,26] lanthanides)[27,28] can emit vivid colors at specific excitation wavelengths.[29–33] Whether from monochromatic fluorescence to multicolored fluorescence or from static luminescence to dynamic discoloration, fluorescent anti-counterfeiting materials have made significant progress.[34–37] However, materials designed to prevent counterfeiting that rely on more than a single optical mode have not been adequately addressed in information security.

Y. Sun, X. Le, H. Shang, Y. Shen, Y. Wu, T. Chen
Key Laboratory of Marine Materials and Related Technologies
Zhejiang Key Laboratory of Marine Materials and Protective Technologies
Ningbo Institute of Material Technology and Engineering
Chinese Academy of Sciences
Ningbo 315201, China
E-mail: lexiaoxia@nimte.ac.cn; tao.chen@nimte.ac.cn

Y. Sun, X. Le, H. Shang, Y. Shen, Y. Wu, T. Chen
School of Chemical Sciences
University of Chinese Academy of Sciences
19A Yuquan Road, Beijing 100049, China

The ORCID identification number(s) for the author(s) of this article can be found under https://doi.org/10.1002/adma.202401589

DOI: 10.1002/adma.202401589

Q. Liu
Hunan Provincial Key Laboratory of Advanced Materials for New Energy Storage and Conversion
Hunan University of Science and Technology
Xiangtan 411201, China

P. Théato
Soft Matter Synthesis Laboratory
Institute for Biological Interfaces III
Karlsruhe Institute of Technology
Hermann-von-Helmholtz-Platz 1, 76344 Eggenstein-Leopoldshafen, Germany

P. Théato
Institute for Chemical Technology and Polymer Chemistry
Karlsruhe Institute of Technology
Engesser Str.18, 76131 Karlsruhe, Germany

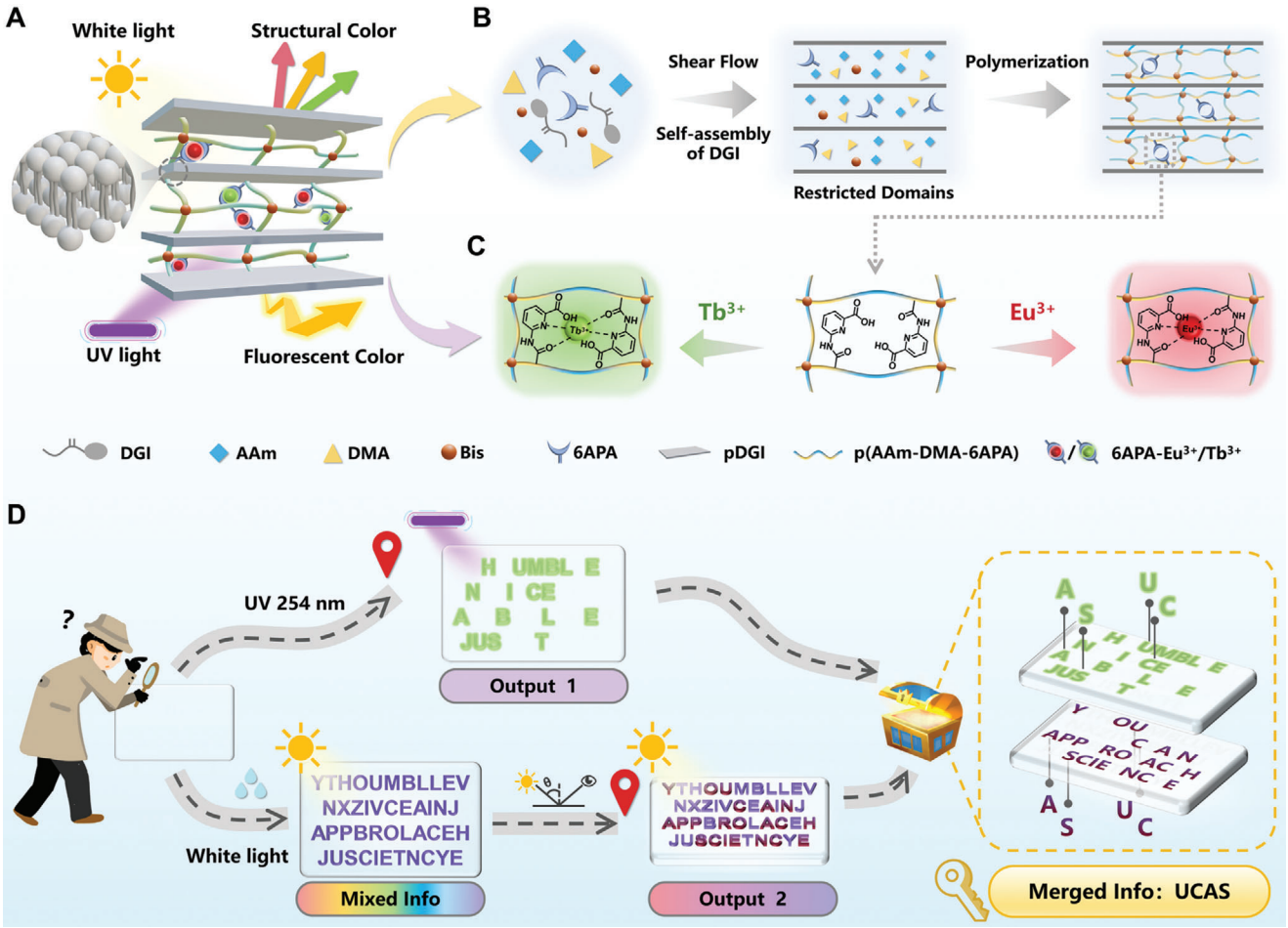

Scheme 1. Dual-mode hydrogel for multistage information encryption. A) Structure diagram of dual-mode hydrogel. B) The preparation of pDGI/p(AAm-DMA-6APA) hydrogel, including the processes of self-assembly and photopolymerization. C) The coordination process of Ln^{3+} and pDGI/p(AAm-DMA-6APA) hydrogel leads to various fluorescence emissions. D) Schematic of dual-mode hydrogel for multistage information encryption.

Constructing non-interference dual- or multi-optical modes materials is an effective strategy for achieving higher levels of information security.[38–40] For instance, Yu and her coworkers[41] reported a dual-mode ink composed of fluorescent cholesteric liquid crystal microdroplets, which can be used to construct security labels showing different messages in the reflective and fluorescent state, respectively. Wang and his colleagues[42] incorporated chemical units (lanthanide-doped fluorophores and phosphors) into colloidal photonic crystals and prepared a large-area photonic film, which exhibits three distinct optical states, i.e., structural color under white light, fluorescent color under UV light (365 nm) and phosphorescent color after turning off UV light. Unlike traditional single-mode anti-counterfeiting strategies, these elegant attempts at dual- or multi-optical modes can increase the capacity of encoded information, improve the difficulty of decryption, and thus enhance the security of information. However, the currently available dual-mode materials have limitations in the multistage encryption process. These limitations include insufficient stimulus responsiveness, the inability to independently modulate structural and fluorescent colors, and the presence of only a single fluorescent color. Therefore, it is of great significance to design an anti-counterfeiting material with independently adjustable and stimulus-responsive properties for multistage secure information anti-counterfeiting systems.[43,44]

Herein, we presented a new strategy to construct a dual-mode hydrogel with both independently tunable structural and fluorescent colors toward multistage information encryption (**Scheme** 1A). In this designable hydrogel system, a rigid lamellar structure of pDGI formed by shear flow-induced self-assembly can provide the restricted domains wherein monomers of acrylamide (AAm) and *N,N'*-Dimethylacrylamide (DMA) underwent polymerization to form a three-dimensional (3D) hydrogel network (Scheme 1B), producing highly responsive structural color. Furthermore, the fluorescent monomer 6APA was incorporated as a site for complexation, allowing coordination with lanthanide ions (Eu^{3+} or Tb^{3+}), which facilitated the achievement of multicolored fluorescence (Scheme 1C). The hydrogel's angle-dependent structural color can be controlled by adjusting the crosslinking density during the formation of restricted domains, as well as a highly responsive to water or moisture.

The responsive structural color can be tuned over a wide color gamut by changing the viewing angle, crosslinking density, and

water content of the hydrogel. Additionally, the multiple fluorescent colors can be modulated by changing the proportion of lanthanide ions. It is worth mentioning that the structural and fluorescent colors are realized as two independent channels that do not interfere with each other. Moreover, through a clever design, the structural color information and the fluorescent color information can be synergistically overlayed to enable a read-out of the final information. Therefore, this dual-mode hydrogel has a robust information storage capacity and coding capacity, allowing for multistage secure information encryption and programable decryption (Scheme 1D). This strategy holds tremendous potential as a platform for encrypting and safeguarding valuable and authentic information in the field of anti-counterfeiting.

2. Results and Discussion

2.1. Fabrication and Characterization of Dual-Mode Hydrogel

The amphipathic monomer dodecylglyceryl itaconate (DGI) (Scheme S1, Supporting Information) and fluorescent ligand 6APA (Scheme S2, Supporting Information) were first prepared according to a previous report,[45] and their successful synthesis was confirmed by ^{1}H NMR spectroscopy (Figures S1–S3, Supporting Information). Using AAm, DMA, DGI and 6APA as monomers, *N*,*N*′-methylenebisacrylamide (Bis). as a crosslinker, diphenyl(2,4,6-trimethylbenzoy)phosphineoxide (TPO) as an initiator, and sodium dodecyl sulfate (SDS) as a surfactant, the precursor solution was stabilized in a warm condition (55 °C) and self-assembled to form lamellar bilayers. Before photopolymerization, this precursor solution was injected into a reaction cell composed of parallel glass plates spaced 0.5 mm apart to produce the DGI lamellar bilayer's-oriented structure (Scheme S3, Supporting Information). The structural color hydrogel pDGI/p(AAm-DMA-6APA) was obtained after being exposed to UV light (365 nm, 20 W) for 3 h at 55 °C. Hydrogels with dual-mode properties were then acquired by immersing the structural color hydrogel in lanthanide metal ion (Ln^{3+}) solutions (0.1 M) (Figure S4, Supporting Information). Since DMA is amphiphilic, the structural color of the hydrogel gradually weakened or even disappeared with the increase of DMA content (Figure S5, Supporting Information), which destroyed the long-range ordered lamellar structure of DGI (Figure S6, Supporting Information). Therefore, we chose a molar ratio of 8:2 for AAm and DMA as the optimal monomer ratio, in which the structural color remained vivid and also provided the possibility for the subsequent introduction of fluorescent monomers. The effect of fluorescent monomer 6APA on the structural color was also explored either with or without lanthanide metal ions, but the colors remain unchanged due to the small content (Figure S7, Supporting Information). Furthermore, the structural color of hydrogels was regulated by changing the content of the crosslinker (1.8 mg, 2 mg, 4 mg, 8 mg, 12 mg, and 16 mg), and the hydrogels were named $LH_{1.8}$, LH_2, LH_4, LH_8, LH_{12}, LH_{16} (Table S1, Supporting Information). Here, LH_2 was taken as an example to conduct the following study.

To confirm the chemical composition and structure of the pDGI/p(AAm-DMA-6APA) hydrogel, we performed attenuated total reflection Fourier transform infrared spectroscopy (ATR-FTIR) and compared it with p(AAm-DMA-6APA) hydrogel. As shown in Figure S8 (Supporting Information), the pDGI/p(AAm-DMA-6APA) hydrogel (red line) shows stretching vibration peaks and vibration peaks of saturated C-H, as well as stretching vibration peaks of the C-O bond, proving the existence of pDGI. Furthermore, compared with p(AAm-DMA-6APA) hydrogel, the storage modulus (G′) and loss modulus (G″) of pDGI/p(AAm-DMA-6APA) hydrogel were enhanced by an order of magnitude due to the introduction of oriented pDGI bilayers (Figure S9, Supporting Information). Similarly, both the elongation at break and the breaking strength of pDGI/p(AAm-DMA-6APA) hydrogel were three times higher than the p(AAm-DMA-6APA) hydrogel. The elastic modulus of pDGI/p(AAm-DMA-6APA) hydrogel was higher than that of p(AAm-DMA-6APA) hydrogel, while the tensile modulus was slightly lower than that of p(AAm-DMA-6APA) hydrogel (Figures S10 and S11, Supporting Information). The typical layered microstructure in pDGI/p(AAm-DMA-6APA) hydrogel can be observed by scanning electron microscopy (SEM) (Figure S12, Supporting Information). The orientation of the bilayer structure was further characterized by small-angle X-ray scattering (SAXS) parallel to the bilayer plane. As shown in Figures S13 and S14 (Supporting Information), a clear anisotropic diffraction pattern can be seen at an azimuth of 90°. In addition, the layer space of ≈44.85 nm that was calculated from the equation $2\Pi/d = 0.14$ can be obtained through the relationship of scattering intensity and scattering vector (Figure S15, Supporting Information). All the above results proved the existence of the lamellar structure in pDGI/p(AAm-DMA-6APA) hydrogel.

2.2. The Regulation of Structural Color of pDGI/p(AAm-DMA-6APA) Hydrogel

According to Bragg's diffraction law, the structural color of the hydrogels was determined by the lamellar distances, which can be adjusted by the crosslinking density of the p(AAm-DMA-6APA) network and the water amount. As demonstrated in **Figure 1A**, with the increase of crosslinking density, the swelling degree of the hydrogels decreased, leading to the smaller bilayer spacing (d) and thus a blue-shift of structural colors. An interesting phenomenon was that when the content of the crosslinker was less than 2 mg, the prepared hydrogel exhibited a second-order reflection.[46–49] This phenomenon was because the wavelength of the first-order reflection exceeded the range of visible wavelengths and reached the near-infrared light region, at which time the color of the hydrogel was dominated by the wavelength of the second-order reflection (Figure S16, Supporting Information). According to the Bragg's diffraction law, $2d\sin(\alpha) = n\lambda$. The second-order reflection, i.e., when n = 2, λ_{second} is one-half of λ_{first}, and at this time, the secondary peak of the second-order reflection was in the range of visible wavelengths, and the hydrogel exhibited the corresponding structural color. Interestingly, as the observation angle θ increased, λ moved toward the lower wavelength range, at which time the structural color of the hydrogel was again determined by the main peak of the first-order reflection that moved toward the lower wavelength range and appeared red (Figure S17, Supporting Information). For instance, when the viewing angle was perpendicular to the hydrogel, the structural color of $LH_{1.8}$ was the same as that of LH_{16}, and their

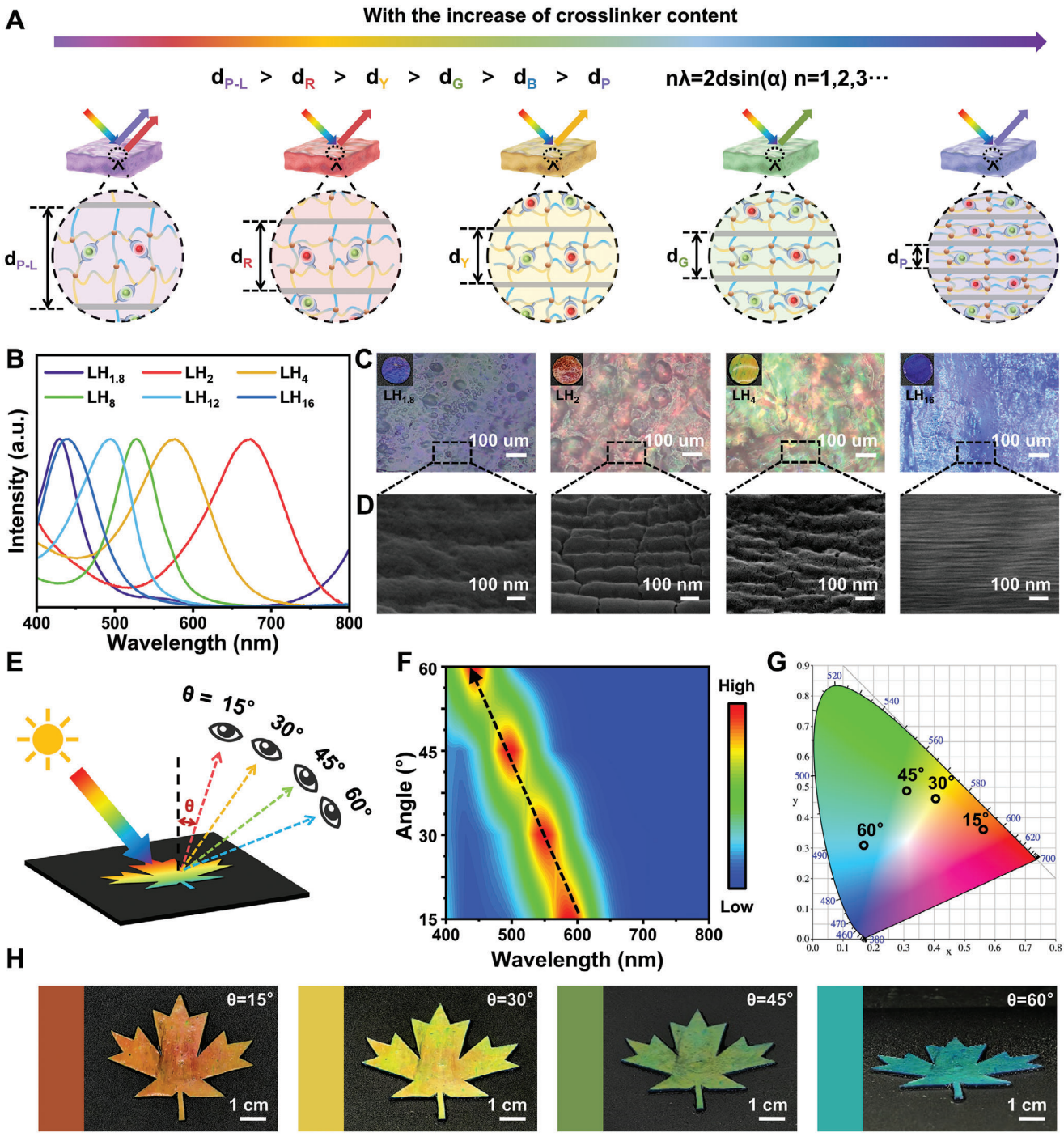

Figure 1. Structural color of pDGI/p(AAm-DMA-6APA) hydrogels regulated by the content of crosslinker and viewing angle. A) Schematic of the structural color and internal structure of pDGI/p(AAm-DMA-6APA) hydrogels prepared with different contents of crosslinker. B) Reflection spectra of pDGI/p(AAm-DMA-6APA) hydrogels ($LH_{1.8}$, LH_2, LH_4, LH_8, LH_{12}, LH_{16}). C) Reflection optical micrographs, photographs (inset), and D) SEM images of $LH_{1.8}$, LH_2, LH_4, LH_{16} hydrogels (viewing angle $\theta = 15°$). E) Schematic diagram of LH_2 observed at different angles (15°–60°). F) Contour maps of angle-dependent reflection spectra, G) CIE chromaticity coordinates, and H) photographs of LH_2 ranging from 15° to 60°.

reflection spectra almost coincided (Figure 1B). According to the digital photos and refection optical micrographs (Figure 1C), we could also see that as the crosslinker content increased, the vivid color of hydrogel varied from blue-purple to red, to yellow-green, and finally to blue-purple. In addition, SEM images directly confirmed that the bilayer spacing (d) decreased with the increase of crosslinker content (Figure 1D; Figure S18, Supporting Information).

To investigate whether the hydrogel shows an angle-dependent reflection, LH_2 was observed at different viewing angles under

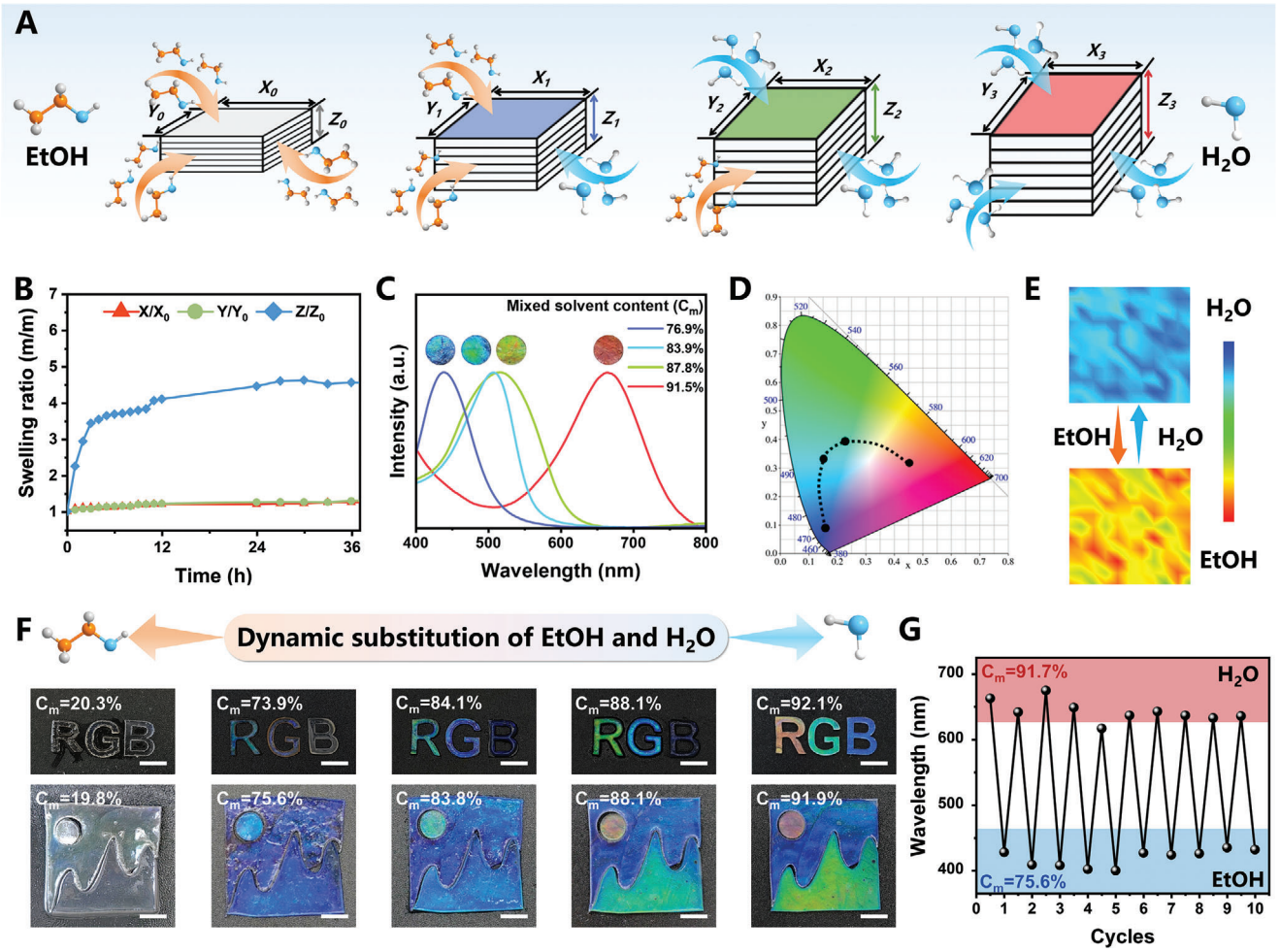

Figure 2. Structural color of pDGI/p(AAm-DMA-6APA) hydrogels adjusted by solvent displacement process between ethanol and water. A) Schematic of the structural color and internal structure of LH_2 with changing EtOH/H_2O mixed solvent content. B) Swelling ratio of LH_2 along the thickness axis (perpendicular to the bilayers, Z/Z_0), along the length axis (parallel to the bilayers, X/X_0), and along the width axis (parallel to the bilayers, Y/Y_0). C) Reflection spectra and D) CIE diagram of LH_2 with different amounts of the mixed solvent content. E) 2D scan images of Fourier infrared spectra when the hydrogel was filled with EtOH and H_2O. F) Photographs of letters and pictures made of LH_2 (red), LH_8 (green), and LH_{16} (blue) with different mixed solvent content (C_m). Scale bar: 1 cm. G) The cyclic changes of reflection peaks during the process of solvent displacement.

visible light (Figure 1E). Specifically, the hydrogel was red at an angle of 15° and turned yellow, green, and blue when the angle changed to 30°, 45°, and 60°, respectively (Figure 1H). Simultaneously, the reflection peak blue-shifted with increasing viewing angles according to the black dashed lines (Figure 1F; Figure S19, Supporting Information). Moreover, the CIE chromaticity coordinates of LH_2 in the CIE chromaticity diagram were also changing with the variation of viewing angles (Figure 1G). All the results indicate that this hydrogel exhibits a tunable structural color and obvious angle-dependent performance, which makes it suitable for potential applications in information displays.

Additionally, the structural color can also be regulated by the solvent displacement in the hydrogel after preparation. As illustrated in **Figure** 2A, the swelling degree of the hydrogel was regulated by immersing LH_2, which was completely soluble in water, in a mixture (1:1) of ethanol (bad solvent) and water (good solvent). Due to the solvent substitution process (Figure S20, Supporting Information), the mixture of ethanol and water brought out the water from the interior of the hydrogel, and the hydrogel network gradually shrank with the increase of immersion time, which led to the variation of structural colors. The main reason is that the swelling of the hydrogel can only occur in the direction perpendicular to the layered structure due to the rigid lamellar layers, which changed the layer spacing. The anisotropic swelling behavior was demonstrated in Figure 2B, in which the swelling ratio of LH_2 along the thickness reached four times its initial value, while the length and width remained almost constant. Concomitant with the anisotropic contraction due to solvent displacement, the structural color of hydrogel went from red (C_m = 91.5%) to yellow-green (C_m = 87.8%), blue-green (C_m = 83.9%), and finally to blue (C_m = 76.9%) as shown by the corresponding reflection spectra and the chromaticity coordinates (Figure 2C,D). The SEM images of hydrogel with different mixed solvent content illustrated more visually the reasons for the blue shift in the structural color of the hydrogel structure (Figure S21, Supporting Information). The process of solvent displacement

can be monitored by two-dimensional (2D) Fourier infrared mapping (Figure 2E).

Given that the structural color was gradually appearing and altering during the swelling process and the horizontal size was not changed, the letters "RGB" and a pattern made up of LH_2 (red), LH_8 (green), and LH_{16} (blue) were designed and assembled. As depicted in Figure 2F, the transparent letters and pattern gradually showed the programed colors in the process of replacing the solvent from mixed solvent (EtOH and H_2O) to water, exhibiting the application of such materials in the field of information encryption and decryption. It is important that the variation of structural color accompanying the solvent changes have excellent repeatability and stability (Figure 2G). Moreover, the structural color can also be adjusted by external forces, which reduced the layer spacing between pDGI bilayers by squeezing the soft hydrogel network (Figure S22, Supporting Information).

2.3. The Modulation of Fluorescence Properties of Dual-Mode Hydrogel

To obtain the dual-mode hydrogels, lanthanide metal ions such as Eu^{3+} and Tb^{3+} were introduced into pDGI/p(AAm-DMA-6APA) hydrogels to form 6APA-Ln^{3+} complexes.[50] The successful coordination of Ln^{3+} ions by the 6APA ligand was verified by photoluminescence (PL) mapping spectra, energy-dispersive X-ray spectroscopy (EDS), X-ray photoelectron spectroscopy (XPS), and fluorescence spectra. On the PL mapping spectra, only one emission center at 545 nm (green center) and 615 nm (red center) was seen for pDGI/p(AAm-DMA-6APA-Tb^{3+}) hydrogel and pDGI/p(AAm-DMA-6APA-Eu^{3+}) hydrogel, respectively (**Figure 3A**). Elemental mapping as shown in Figure 3B further corroborated the uniform distribution of Ln^{3+} ions in pDGI/p(AAm-DMA-6APA-Ln^{3+}) hydrogels. For more quantitative proof, XPS was employed to analyze the changes in binding energy before and after complexation. As shown in Figure 3C, the binding energies of Eu^{3+} ions in pDGI/p(AAm-DMA-6APA-Eu^{3+}) hydrogel mainly included excess free Eu^{3+} ($3d_{3/2}$ = 1166.76 eV and $3d_{5/2}$ = 1137.01 eV) and bonded Eu^{3+} ($3d_{3/2}$ = 1156.96 eV and $3d_{5/2}$ = 1125.96 eV). Similarly, the Tb4d spectra of pDGI/p(AAm-DMA-6APA-Tb^{3+}) hydrogel also showed a lower shift in the binding energy after coordination (Figure 3D), which is ascribed to the electron sharing between lanthanide metal ions and N atom or O atom.[51] For the fluorescence color of dual-mode hydrogels, it was modulated by changing the molar ratio of Eu^{3+}/Tb^{3+} in the mixed solutions. When the molar ratio varies from 0:1 to 7:3 and 1:0, the hydrogels corresponded to green, yellow, and red, which was confirmed by the fluorescence spectra (Figure 3E) and CIE coordinates (Figure 3F).

Since both structural and fluorescent colors can be regulated and the dual optical modes are non-interfering, an array pattern (16 × 7) consisting of four kinds of dual-mode hydrogel pixels was fabricated for information anti-counterfeiting (Figure 3G). The array pattern displayed two different information of a green reflective pattern "2023" under visible light and a green fluorescent pattern "0424" under UV light (254 nm). Furthermore, these hydrogel pixels can build the American Standard Code (ASC) for the encoding, encryption, and decryption of information. Specifically, red (either structural or fluorescent color) corresponds to the binary digit "0", while green (either structural or fluorescent color) represents "1" (Figure S23, Supporting Information). To obtain the final message, the word "information" in reflection mode and the phrase "hello world" in fluorescent mode need to be combined, enhancing information security. Similarly, a "four-leaf clover" pattern was encoded with the assistance of ion-printing technology on the dual-mode hydrogels, which could only be decrypted by the correct assembly and exposure to UV irradiation (Figure S24, Supporting Information).

2.4. Dual-Mode Hydrogel for Multistage Information Encryption

Current anti-counterfeiting materials, though effective, have notable limitations. For instance, materials with structural colors offer difficulty in replication but perform poorly in low or no light, limiting their applications. On the other hand, fluorescent materials can conceal information under natural light but can be mimicked by similar colored pigments, diminishing their anti-counterfeiting effectiveness. Moreover, both chemical and structural color-based materials face challenges in encoding ample information with a single optical mode. Consequently, there is a crucial demand for developing anti-counterfeiting technologies that combine multiple optical information modes within a single material to overcome these limitations.[52,53]

Dual or multi-optical mode materials represent a significant leap forward, offering increased information storage, enhanced anti-counterfeiting measures, and higher levels of encryption security. As a proof of concept for multistage information encryption based on dual-mode hydrogels, a random alphabet was designed, as depicted in **Figure 4A**. To increase the difficulty of decryption but receive the final target information, the following two points had to be considered: 1) The alphabet consisted of purple structural color LH_{16} (high crosslinking) and purple $LH_{1.8}$ (low crosslinking) with second-order reflection, of the former acting as interference letters and the latter as carriers for structural color information (Output 2). 2) Specific letters "UCAS" made up of $LH_{1.8}$ and other confusing letters composed of LH_{16} were selected for Tb^{3+} ions treatment.

In the initial state, the hydrogels treated by ethanol were completely transparent but emitted fluorescence (Figures S25 and S26, Supporting Information), so that four words "HUMBLE, NICE, ABLE, JUST" (Output 1) showed under UV light (254 nm) but no information under visible light (Figure 4B). Moreover, the hydrogel maintained its bright structural and fluorescent colors after long-term storage in water (Figure S27, Supporting Information). Once the hydrogels absorbed water and reached swelling equilibrium, a jumble of letters ("Mixed info") with a purple structural color appeared due to the indistinguishable purple color between $LH_{1.8}$ and LH_{16} at a vertical viewing angle. When shifting the viewing angle, $LH_{1.8}$ turned to red, while LH_{16} showed blue-violet, revealing a complete sentence "YOU CAN APPROACH SCIENCE" ("Output 2"). The final encrypted message "UCAS" was obtained by picking out the letters that appear in both "Output 1" and "Output 2". This intriguing result attests to the potential applicability of our dual-mode hydrogels in the realm of anti-counterfeiting technology.

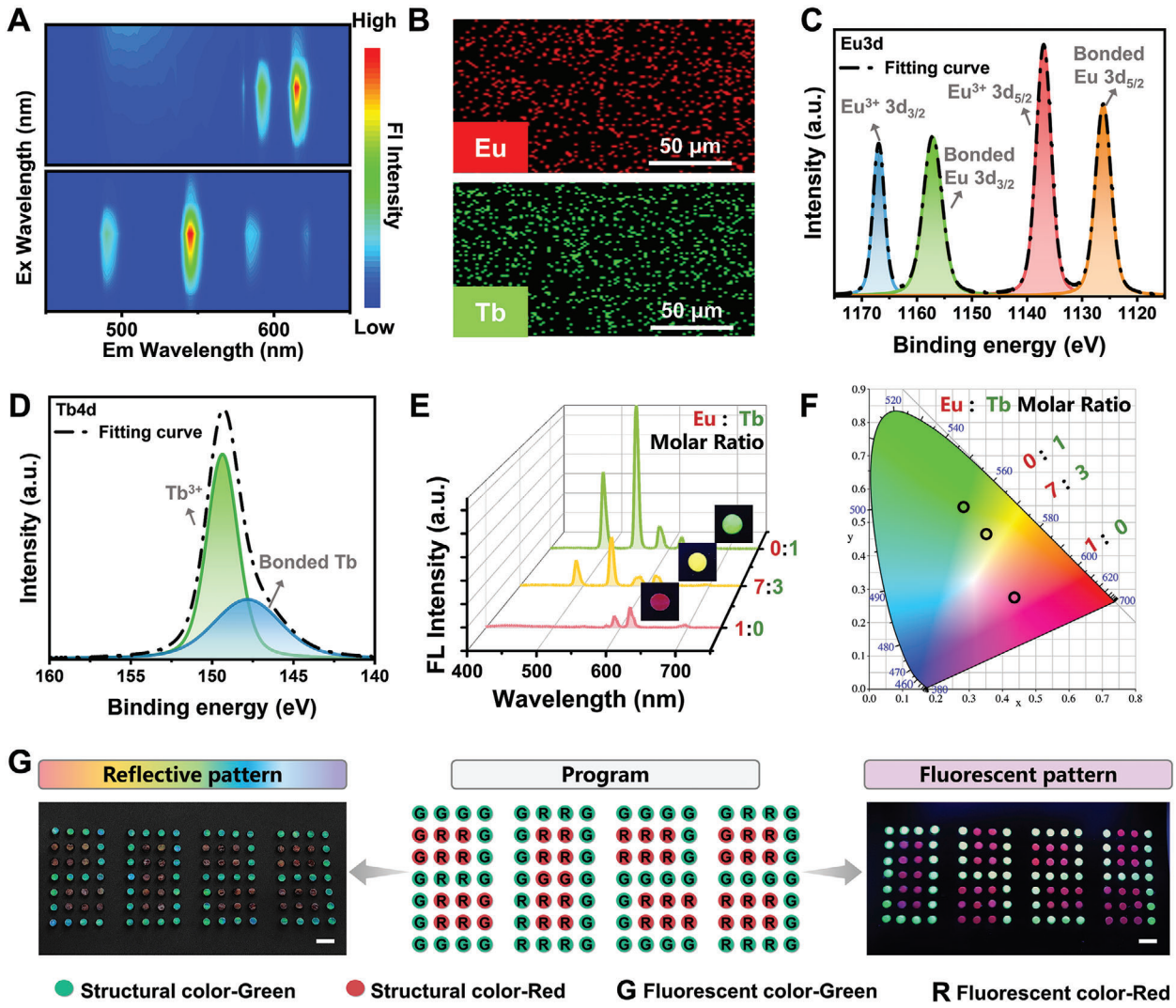

Figure 3. Regulation and characterization of fluorescent properties of dual-mode hydrogel. A) PL mapping spectra of dual-mode hydrogel with Eu^{3+} and Tb^{3+}, respectively. B) EDS mapping of Eu in pDGI/p(AAm-DMA-6APA-Eu^{3+}) hydrogel and Tb in pDGI/p(AAm-DMA-6APA-Tb^{3+}) hydrogel. C) XPS fitting results for Eu3d spectra of pDGI/p(AAm-DMA-6APA-Eu^{3+}) hydrogel. D) XPS fitting results for Tb4d spectra of pDGI/p(AAm-DMA-6APA-Tb^{3+}) hydrogel. E) Fluorescence spectra (λ_{ex} = 254 nm) and F) CIE diagram of dual-mode hydrogels with different Eu: Tb molar ratios. G) An elaborate pattern with two different messages of a green "2023" structural color information and a green "0424" fluorescent color information (scale bar: 1 cm).

3. Conclusion

In summary, a series of dual-mode hydrogels with both independently tunable and fluorescent colors toward multistage secure information encryption was fabricated. These hydrogels consisted of a rigid lamellar structure pDGI, which was formed by shear flow-induced self-assembly. The rigid lamellar structure provided the restricted domains wherein monomers undergo polymerization to form a hydrogel network, resulting in structural color. Moreover, fluorescent monomer 6APA was introduced as a complexation site for coordination with lanthanide ions to achieve multicolor fluorescence. Owing to the adjustable layer spacing of pDGI, the responsive angle-dependent structural color was controlled by adjusting the crosslinking density and water content. In addition, the fluorescent color of hydrogels could be modulated by the molar ratio of Eu^{3+}/Tb^{3+} in aqueous solution. Since the dual optical modes are non-interfering, this kind of material can be applied for storing distinct information, and decrypting hidden information through a programed decryption process, including UV light irradiation, water stimulation, viewing angle variation, and information integration. In a word, this unique dual-mode material with distinct structural and fluorescent colors opens the avenue for promising applications across diverse domains, including information encoding, displaying, and advanced anti-counterfeiting.

4. Experimental Section

Materials: Dodecylglyceryl itaconate (DGI) was synthesized according to the previous report.[47] The crude product was purified in a silica gel column and eluted with a hexane/ethyl

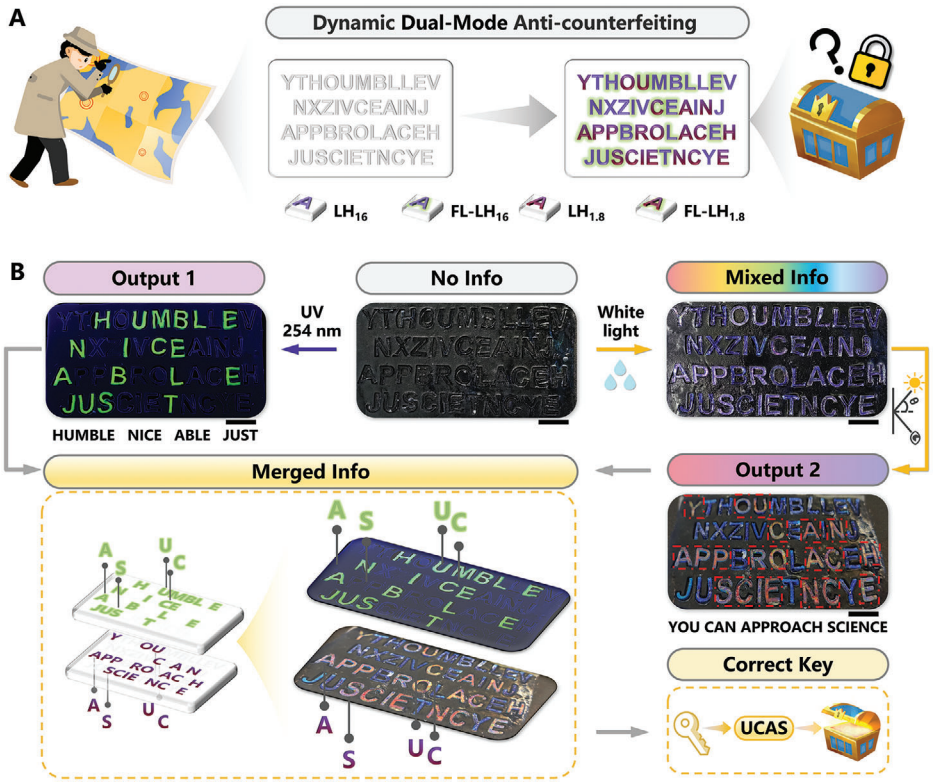

Figure 4. Dual-mode hydrogels for multistage information encryption. A) Schematic diagram of designing complex encrypted information based on dual-mode hydrogels. B) Final information "UCAS" was displayed progressively under the synergy of fluorescent information and angle-dependent structural color information (scale bar: 1 cm).

acetate mixture (volume ratio 1:1). The collected DGI sample was further purified twice by recrystallization in a mixed solution of acetone and hexane (mass ratio 1:1). Fluorescent ligand 6APA was synthesized according to the previous reports.[52] Acrylamide (AAm), *N,N′*-Dimethylacrylamide (DMA), *N,N′*-methylenebisacrylamide (Bis), diphenyl(2,4,6-trimethylbenzoyl)phosphine oxide (TPO), Sodium dodecyl sulfate (SDS), $Eu(NO_3)_3{\cdot}6H_2O$, and $Tb(NO_3)_3{\cdot}5H_2O$ were purchased from Aladdin Chemical Co.

Fabrication of pDGI/p(AAm-DMA-6APA) Hydrogel: First, DGI (150 mg), AAm (576 mg), DMA (0.205 mL), 6APA (1.23 mg), SDS (0.16 mg), Bis (1.8 mg–16 mg), and TPO (3 mg) were added and dissolved in deionized water (5 mL) at 55 °C for 24 h to form stable lamellar bilayers. After being purged in a nitrogen atmosphere to remove dissolved oxygen, the precursor solution was injected into a simple polymerization cell that was made up of two glass sheets (8 cm × 8 cm) and one PDMS mold (0.5 mm). Finally, the oriented bilayer was stabilized under UV irradiation (365 nm, 20 W) at a temperature of 55 °C for 3 h. The prepared hydrogel was immersed in deionized water for 1 week to reach swelling equilibrium as well as remove unreacted chemicals.

Fabrication of Dual-Mode pDGI/p(AAm-DMA-6APA-Ln^{3+}) Hydrogel: According to the previous work, the optimal coordination ratio of fluorescent monomer 6APA and lanthanide metal ions is 2:1.[50–54] Therefore, it was chosen to immerse pDGI/p(AAm-DMA-6APA) hydrogel with an excess concentration of $Ln(NO_3)_3$ solution to realize the effect of complete coordination. Specifically, the dual-mode pDGI/p(AAm-DMA-6APA-Ln^{3+}) hydrogel was obtained by immersing pDGI/p(AAm-DMA-6APA) hydrogel in $Eu(NO_3)_3$ or $Tb(NO_3)_3$ (0.1 M) solution for 15 min at room temperature. By adjusting the ratio of Eu^{3+} and Tb^{3+}, the fluorescence color of the hydrogel can be transformed into red, yellow, and green. Then, the pDGI/p(AAm-DMA-6APA-Ln^{3+}) hydrogel was placed in deionized water to remove uncoordinated Ln^{3+}. Based on the theoretical values, the concentration of the coordinated Ln^{3+} in the hydrogel was calculated to be $\approx 3.2 \times 10^{-3}$ mmol.

Characterization: ^{1}H NMR spectra were obtained from a Bruker Avance III 400 MHz spectrometer. UV–vis absorption and transmittance spectra were measured on a UV-Vis spectrophotometer (TU-1810, Purkinje General Instrument Co. Ltd.). ATR-FTIR spectra were recorded on a Thermo Scientific Nicolet 6700 FT-IR spectrometer. The digital photos of the hydrogel were taken under a UV lamp (ZF-5, 5 W, 254 nm). Fluorescent intensity was recorded with a HPRIBA FL3-111 fluorescence spectrometer. The reflectance spectra were acquired on a PerkinElmer Lambda 950 spectrometer with a relative mirror reflection attachment with a variable angle. SEM images were taken by scanning electron microscope (S-4800, Hitachi). TEM images were taken with a transmission electron microscope (F20, Tecnai). The SAXS of hydrogels were measured by Xeuss 3.0 UHR. Rheological characterization was carried out on a stress-controlled rheometer (TA-dhr2) with a parallel plate (25 mm) in frequency sweep mode (from 0.1 to 100 rad s^{-1}) at a constant shear strain of 1%.

Supporting Information

Supporting Information is available from the Wiley Online Library or from the author.

Acknowledgements

This work was supported by the National Key R&D Program of China (2022YFB3204300), the National Natural Science Foundation of China (52103246), Zhejiang Provincial Natural Science Foundation of China (LD22E050008 and LQ22E030015), Natural Science Foundation of Ningbo

(2023J408 and 20221JCGY010301), Ningbo International Cooperation Project (2023H019), and the Sino-German Mobility Program (M-0424).

Conflict of Interest

The authors declare no conflict of interest.

Data Availability Statement

The data that support the findings of this study are available in Supporting Information of this article.

Keywords

anti-counterfeiting, dual-mode information, encryption-decryption, fluorescent hydrogel, structural color

Received: January 30, 2024
Revised: May 10, 2024
Published online:

[1] B. Yoon, J. Lee, I. S. Park, S. Jeon, J. Lee, J. M. Kim, *J. Mater. Chem. C* **2013**, *1*, 2388.
[2] R. Arppe, T. J. Sørensen, *Nat. Rev. Chem.* **2017**, *1*, 0031.
[3] P. Kumar, S. Singh, B. K. Gupta, *Nanoscale* **2016**, *8*, 14297.
[4] Y. Li, P. Gao, *Chemosensors* **2023**, *11*, 489.
[5] J. Hou, M. Li, Y. Song, *Angew. Chem., Int. Ed.* **2018**, *57*, 2544.
[6] L. Shang, W. Zhang, K. Xu, Y. Zhao, *Mater. Horiz.* **2019**, *6*, 945.
[7] M. M. Ito, A. H. Gibbons, D. Qin, D. Yamamoto, H. Jiang, D. Yamaguchi, K. Tanaka, E. Sivaniah, *Nature* **2019**, *570*, 363.
[8] B. H. Miller, H. Liu, M. Kolle, *Nat. Mater.* **2022**, *21*, 1014.
[9] X. Lin, D. Shi, G. Yi, D. Yu, *Responsive Mater.* **2024**, *2*, 20230031.
[10] K. J. Vahala, *Nature* **2003**, *424*, 839.
[11] J. Ge, Y. Yin, *Angew. Chem., Int. Ed.* **2011**, *50*, 1492.
[12] S. Tokunaga, Y. Itoh, H. Tanaka, F. Araoka, T. Aida, *J. Am. Chem. Soc.* **2018**, *140*, 10946.
[13] L. Zhu, C. Xu, P. Chen, Y. Zhang, S. Liu, Q. Chen, S. Ge, W. Hu, Y. Lu, *Light Sci. Appl.* **2022**, *11*, 135.
[14] H. K. Bisoyi, Q. Li, *Chem. Rev.* **2016**, *116*, 15089.
[15] T. H. Zhao, G. Jacucci, X. Chen, D. Song, S. Vignolini, R. M. Parker, *Adv. Mater.* **2020**, *32*, 2002681.
[16] Q. Guo, Y. Li, Q. Liu, Y. Li, D. Song, *Angew. Chem., Int. Ed.* **2022**, *61*, 202113759.
[17] B. E. Droguet, H. Liang, B. Frka-Petesic, R. M. Parker, M. F. L. De Volder, J. J. Baumberg, S. Vignolini, *Nat. Mater.* **2022**, *21*, 352.
[18] R. M. Parker, T. H. Zhao, B. Frka-Petesic, S. Vignolini, *Nat. Commun.* **2022**, *13*, 3378.
[19] H. Hu, X. Zhang, W. Liu, Q. Hou, Y. Wang, *Chem. Eng. J.* **2023**, *474*, 145980.
[20] Q. Tan, D. Li, L. Li, Z. Wang, X. Wang, Y. Wang, F. Song, *Nano Lett.* **2023**, *23*, 9841.
[21] D. Li, J. Wu, Z. Liang, L. Li, X. Dong, S. Chen, T. Fu, X. Wang, Y. Wang, F. Song, *Adv. Sci.* **2023**, *10*, 2206290.
[22] S. N. Baker, G. A. Baker, *Angew. Chem., Int. Ed.* **2010**, *49*, 6726.
[23] H. Yang, Y. Liu, Z. Guo, B. Lei, J. Zhuang, X. Zhang, Z. Liu, C. Hu, *Nat. Commun.* **2019**, *10*, 1789.
[24] S. Wu, H. Shi, W. Lu, S. Wei, H. Shang, H. Liu, M. Si, X. Le, G. Yin, P. Theato, T. Chen, *Angew. Chem., Int. Ed.* **2021**, *60*, 21890.
[25] H. N. Kim, M. H. Lee, H. J. Kim, J. S. Kim, J. Yoon, *Chem. Soc. Rev.* **2008**, *37*, 1465.
[26] L. Ding, X. Wang, *J. Am. Chem. Soc.* **2020**, *142*, 13558.
[27] K. Binnemans, *Chem. Rev.* **2009**, *109*, 4283.
[28] J. Rocha, L. D. Carlos, F. A. A. Paz, D. Ananias, *Chem. Soc. Rev.* **2011**, *40*, 926.
[29] Q. Wang, Q. Zhang, Q. Zhang, X. Li, C. Zhao, T. Xu, D. Qu, H. Tian, *Nat. Commun.* **2020**, *11*, 158.
[30] Z. Li, X. Ji, H. Xie, B. Z. Tang, *Adv. Mater.* **2021**, *33*, 2100021.
[31] J. Zhang, B. He, Y. Hu, P. Alam, H. Zhang, J. W. Y. Lam, B. Z. Tang, *Adv. Mater.* **2021**, *33*, 2008071.
[32] Z. Zong, Q. Zhang, S. Qiu, Q. Wang, C. Zhao, C. Zhao, H. Tian, D. Qu, *Angew. Chem., Int. Ed.* **2022**, *61*, 202116414.
[33] M. Lei, Q. Wang, R. Gu, D. Qu, *Responsive Mater.* **2024**, *2*, 20230027.
[34] Z. Xie, X. Zhang, H. Wang, C. Huang, H. Sun, M. Dong, L. Ji, Z. An, T. Yu, W. Huang, *Nat. Commun.* **2021**, *12*, 3522.
[35] Y. Jiang, J. Ma, Z. Ran, H. Zhong, D. Zhang, N. Hadjichristidis, *Angew. Chem., Int. Ed.* **2022**, *61*, 202208516.
[36] Q. Wang, B. Lin, M. Chen, C. Zhao, H. Tian, D. Qu, *Nat. Commun.* **2022**, *13*, 4185.
[37] K. Zhang, X. Zhou, S. Li, L. Zhao, W. Hu, A. Cai, Y. Zeng, Q. Wang, M. Wu, G. Li, J. Liu, H. Ji, Y. Qin, L. Wu, *Adv. Mater.* **2023**, *35*, 2305472.
[38] B. B. Patel, D. J. Walsh, D. H. Kim, J. Kwok, B. Lee, D. Guironnet, Y. Diao, *Sci. Adv.* **2020**, *6*, eaaz7202.
[39] R. Chen, D. Feng, G. Chen, X. Chen, W. Hong, *Adv. Funct. Mater.* **2021**, *31*, 2009916.
[40] X. Lai, Q. Ren, F. Vogelbacher, W. E. I. Sha, X. Hou, X. Yao, Y. Song, M. Li, *Adv. Mater.* **2022**, *34*, 2107243.
[41] L. Qin, X. Liu, K. He, G. Yu, H. Yuan, M. Xu, F. Li, Y. Yu, *Nat. Commun.* **2021**, *12*, 699.
[42] H. Huang, H. Li, J. Yin, K. Gu, J. Guo, C. Wang, *Adv. Mater.* **2023**, *35*, 2211117.
[43] Y. Sun, X. Le, S. Zhou, T. Chen, *Adv. Mater.* **2022**, *34*, 2201262.
[44] Y. Shen, X. Le, Y. Wu, T. Chen, *Chem. Soc. Rev.* **2024**, *53*, 606.
[45] K. Tsujii, M. Hayakawa, T. Onda, T. Tanaka, *Macromolecules* **1997**, *30*, 7397.
[46] R. Colombelli, K. Srinivasan, M. Troccoli, O. Painter, C. F. Gmachl, D. M. Tennant, A. M. Sergent, D. L. Sivco, A. Y. Cho, F. Capasso, *Science* **2003**, *302*, 1374.
[47] G. Maisons, M. Carras, M. Garcia, B. Simozrag, X. Marcadet, *Appl. Phys. Lett.* **2011**, *98*, 021101.
[48] T. Shen, S. Hong, B. Lee, J. Song, *NPG Asia Mater.* **2016**, *8*, e296.
[49] H. S. Kang, S. W. Han, C. Park, S. W. Lee, H. Eoh, J. Baek, D. G. Shin, T. H. Park, J. Huh, H. Lee, D. E. Kim, D. Y. Ryu, E. L. Thomas, W. G. Koh, C. Park, *Sci. Adv.* **2020**, *6*, eabb5769.
[50] S. Wei, W. Lu, X. Le, C. Ma, H. Lin, B. Wu, J. Zhang, P. Theato, T. Chen, *Angew. Chem.* **2019**, *131*, 16389.
[51] H. Shi, S. Wu, M. Si, S. Wei, G. Lin, H. Liu, W. Xie, W. Lu, T. Chen, *Adv. Mater.* **2022**, *34*, 2107452.
[52] H. Wang, Y. Tang, Z. Huang, F. Wang, P. Qiu, X. Zhang, C. Li, Q. Li, *Angew. Chem., Int. Ed.* **2023**, *62*, 202313728.
[53] L. Wang, Q. Li, *Chem. Soc. Rev.* **2018**, *47*, 1044.
[54] X. Le, H. Shang, S. Gu, G. Yin, F. Shan, D. Li, T. Chen, *Chin. J. Chem.* **2022**, *40*, 337.